International Atomic Energy Agency

INDC(SLK)-002
Distr.: L

INDC INTERNATIONAL NUCLEAR DATA COMMITTEE

CROSS SECTIONS OF THE $^{16}O(n,\alpha\gamma)$ REACTION AT 14.7 MeV

S. Hlaváč, P. Obložinský, I. Turzo, L. Dostál and J. Kliman
Institute of Physics, Slovak Academy of Sciences
842 28 Bratislava, Slovakia

(Final Report for IAEA Research Contract No. 6970/RB)

August 1994

INDC(SLK)-002
Distr.: L

CROSS SECTIONS OF THE $^{16}O(n,\alpha\gamma)$ REACTION AT 14.7 MeV

S. Hlaváč, P. Obložinský, I. Turzo, L. Dostál and J. Kliman
Institute of Physics, Slovak Academy of Sciences
842 28 Bratislava, Slovakia

(Final Report for IAEA Research Contract No. 6970/RB)

August 1994

Reproduced by the IAEA in Austria
August 1994

CONTENTS

1 Introduction

Cross sections for production of charged particles in fast neutron interactions are of recent interest in view of their importance in the conceptual and technical design of fusion reactors. This interest is emphasized also by the International Atomic Energy Agency in Vienna via its current Coordinated Research Program "Improvement of neutron induced helium production cross sections".

Cross section of the reaction $^{16}O(n,\alpha)^{13}C$ is relevant for a specific reason. An important characteristic of a fusion reactor is the neutron multiplication in the reactor wall. The reactor wall is a complex structure with different components, one of those being made of Be. Neutrons are multiplied partly in the reactor blanket via (n,2n) reaction on Be. Neutron multiplication constant is usually determined experimentally in a manganese bath. For precise determination of this constant, careful analysis of neutron interaction in the whole experimental setup is necessary. One of the important points is the neutron interaction with water, especially elastic and inelastic interaction with oxygen. Apart from elastic scattering on oxygen, neutrons undergo also (n,α) reaction with ^{16}O and are thus lost for the multiplication process. Therefore a good knowledge of the cross section for this reaction is necessary. Requested precision of the (n,α) cross section is better than 10% [1].

At present, the cross section of $^{16}O(n,\alpha)$ in the 14 MeV neutron energy range is known to about 20-30%. Direct measurement of α particle production is rather tedious and only several measurements were performed so far, the most recent and most complete by Bormann[3]. From these measurements follow that only a small part of the cross section goes through the α_0 channel directly to the ground state of the final nucleus ^{13}C. Borman's results [3] show that more than 80% of the intensity goes to the excited levels that depopulate afterwards via γ decay. This opens up a new possibility for cross section measurements. Instead of the α particle production measurement, one can determine population of excited levels due to (n,α) reaction by measuring γ rays emitted after discrete level depopulation.

Production cross section of 2 prominent γ lines with energies 3684.4 keV and 3853.6 keV is reported in the literature. To our knowledge, around 10 measurements of discrete γ ray production in $^{16}O(n,\alpha\gamma)$ were performed so far. However, the situation with existing experimental data is highly unpleasant. Most of the measurements were done several decades ago using low resolution Na(Tl) spectrometers or Ge(Li) detectors with very low efficiency and rather bulky samples. At the incident neutron energies around 14-15 MeV the literature data show rather great discrepancies. For the 3684.4 keV transition at 14.5 MeV the cross sections vary from 20 mb to 65 mb. The situation with the 3853.6 keV transition is similar and the observed differences could be expressed by a factor of 3.

In our laboratory, we recently developed highly specialized system suitable for photon production measurement in 14 MeV neutron induced reactions. It consists of a continuous 14 MeV neutron generator, associated α particle system for timing purposes and neutron flux determination, and variety of photon detectors for continuous as well as discrete photon energy ranges. Due to that we found it possible to perform precise up-to-date measurement of $^{16}O(n,\alpha\gamma)$ cross section.

In the following paragraphs, we describe first the experiment, then we proceed to the

analysis of γ spectra and in the last part we discuss obtained results.

2 Experiment

Measurements were performed at the neutron generator of the Institute of Physics in Bratislava [2]. Schematic view of the experimental setup is shown in Fig.1. The experiment is based on the time-correlated associated particle method and the setup is designed in a way to utilize fully the advantage of strong spatial and time correlations between neutrons and alpha particles for background reduction.

2.1 Experimental setup

A beam of magnetically separated 150 keV D^+ ions bombarded a water cooled TiT target of 4.5 cm diameter. The beam itself was restricted to a diameter of 5 mm by a diaphragm placed close to the target. This diaphragm is very important for correct geometrical adjustment of the whole setup. The beam current at the TiT target was about 50-80 μA.

Neutrons were produced in the TiT target by the T(D,n)α reaction. Associated α particles were detected by a fast plastic scintillation counter placed at an angle of 135° with respect to the D^+ beam. We used fast plastic scintillator, similar to NE102, with thickness of 100 μm and diameter of 4.0 cm. A movable diaphragm with dimensions of 1.5×1.5 cm^2 at the distance of 37.5 cm from the TiT target determined the solid angle of the α particle detector. Transversal movement of this diaphragm allowed fine adjustment of the neutron cone position. The gain of the α particle detector and the threshold were calibrated with a built-in ^{241}Am α source (E_α = 5.5 MeV).

Associated neutrons collimated electronically by α particles flew first through an iron collimator and then through an opening in a combined concrete/polyethylene wall which fully separated neutron source and photon detector. The angle between deuteron beam and the axis of collimated neutron beam was 45° resulting in the mean neutron energy in the cone of 14.7 MeV and an energy spread of about 400 keV.

Sample position at the distance of 270 cm from the TiT target was fixed, but the neutron cone position was experimentally adjusted to the sample position by the movable diaphragm in front of the associated α particle detector. The size of the neutron cone at the sample spot was 14×14 cm^2, thus the samples were always inside the cone, even taking into account possible shifts of the deuteron beam along the TiT target. Behind the sample, a NE213 (ϕ12 cm $\times$4 cm) scintillation detector was located to control the cone position by measuring the ratio of n$\times\alpha$ coincidences to single neutrons.

2.2 HPGe photon detector

Photons emitted from the sample were registered by a HPGe detector, which was placed at the distance of 18.7 cm from the sample and an angle of 125° with respect to the axis of the collimated neutron beam. The angle of 125° was chosen to set the second Legendre polynomial to zero thus avoid problems with unknown angular distribution of γ rays. The detector had a sensitive volume of 244 cm^3 and the FWHM energy resolution of 1.96

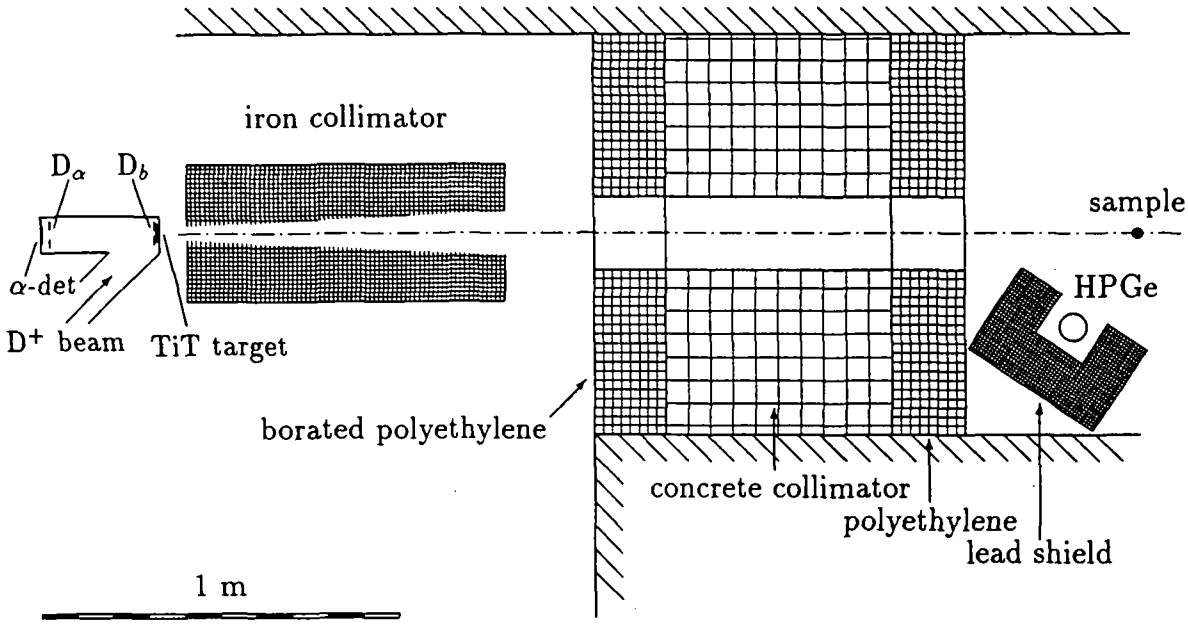

Figure 1: *Simplified sketch of the experimental setup. D_b and D_α denote diaphragms that define the beam spot and the solid angle of the α particle detector, respectively.*

keV at the 1332 keV γ-ray energy. The intrinsic time resolution was rather poor, about 13 ns, due to rather large detector dimensions. The HPGe detector, with axis oriented perpendicularly to the detector - sample direction, was surrounded by a lead shielding in order to further reduce the background caused by scattered neutrons.

The efficiency determination of the HPGe detector up to about 4000 keV was necessary for the present experiment. The only suitable isotopic source with high energy photons close to this energy range is ^{56}Co. The absolute full energy peak efficiencies were measured with calibrated ^{152}Eu, ^{24}Na sources and uncalibrated ^{56}Co source. The ^{24}Na source was prepared by Al foil activation with 14 MeV neutrons during the experiment and its activity was measured with an absolutely calibrated Ge(Li) detector at the IRK Vienna [4]. The relative efficiency for high energy photons measured with ^{56}Co up to 3547 keV was normalized to the low energy points measured with other two sources. During efficiency measurements a few runs were made, with γ-sources located at different points of the sample surface. The final detector efficiency , shown in Fig.2, was obtained by averaging these runs, thus the influence of the sample and detector geometrical sizes were taken into account. The final curve was obtained by fitting the experimental points with the commonly used polynomial function

$$\log \epsilon(E_\gamma) = \sum_{n=0}^{5} p_n \times (\log E_\gamma)^n, \qquad (1)$$

where $\epsilon(E_\gamma)$ is the absolute full energy peak efficiency for photons with the energy E_γ and p_n are fitted coefficients. Efficiency decreases at low energies due to a relatively high

threshold which was necessary to improve the time resolution. In the high energy region the efficiency is sufficiently linear in the log-log plot of Fig.2. This guarantees that the

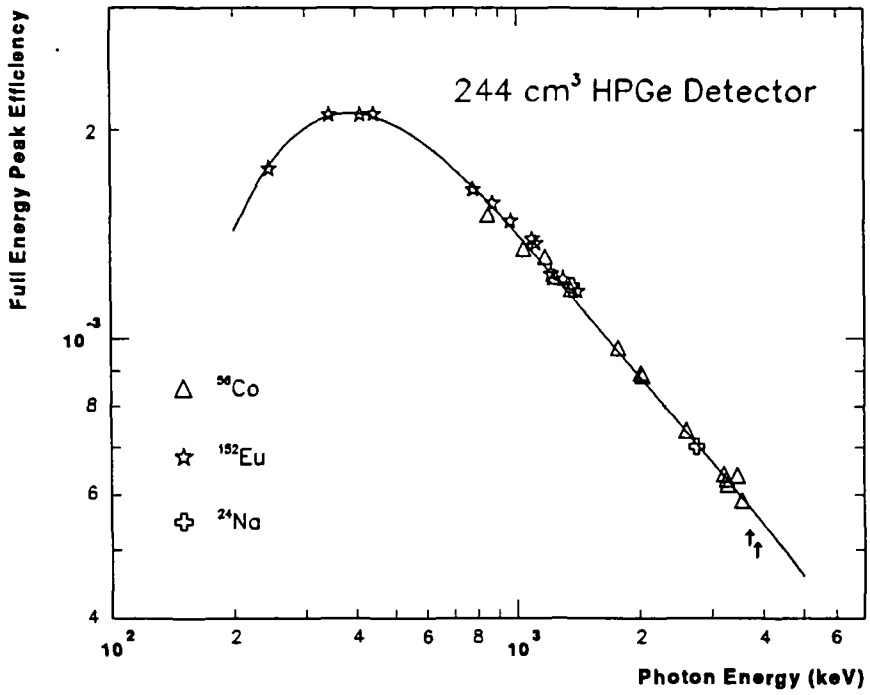

Figure 2: *Absolute full energy peak efficiency for the 244 cm^3 HPGe detector. Detector to source (center to center) distance was 18.6 cm. The line is a fit of eq. 1. to the experimental data. Two arrows bellow 4000 keV denote the energies of two γ transitions for which we extrapolate the measured efficiency.*

required extrapolation from the last experimental point at 3547 keV to 3684 and 3853 keV photon energy, shown by arrows in Fig.2, is plausible.

2.3 Electronics

The block-scheme of electronics is shown in Fig.3. For shaping, timing and logic purposes we used NIM electronics. Data taking was performed using the CAMAC system.

Outputs of both γ and α detectors were splitted to obtain independent time and energy signals. Essential for the whole electronics is fast overlap coincidence (ORTEC-ESN Co4010). This coincidence determined whether a detected γ ray was correlated with an α particle and therefore with a neutron, since we are interested only in prompt γ rays. Moreover, the timing was determined by the α particle detector. Therefore, a HPGe timing signal was formed to have the width of 200 ns, the timing signal of the α detector was kept short ($\sim$ 20 ns) and delayed by such an amount that the correlated α signal arrived in the middle of the HPGe timing pulse. Thus, the timing of the overlap coincidence output was given by the delayed α signal. Dead time (or data acquisition

busy) flag was also fed to this coincidence in anticoincidence mode to prevent a new interrupt until the old event was finished. Output of the overlap coincidence started both TDCs, opened gates for all analog signals and after same delay (100 μs to allow for data digitalization) generated LAM in the CAMAC system.

Energy signal from HPGe goes via a shaping amplifier (Silena 7400) to the NIM ADC (ND 8102) and the ND-CAMAC interface. Time signal is shaped in a timing filter

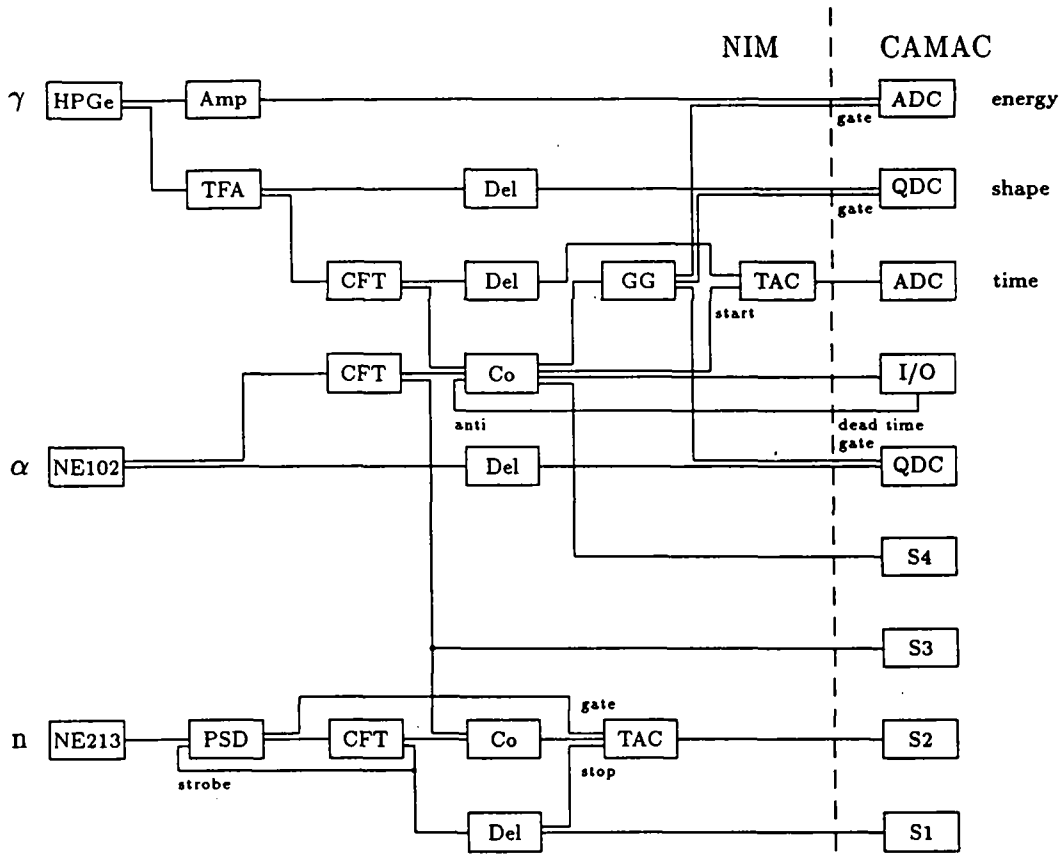

Figure 3: *Simplified block scheme of the electronics. NIM and CAMAC electronics is separated by a dash line. The abbreviations represent following electronic modules: Amp - shaping amplifier, TFA - timing filter amplifier, CFT - constant fraction timing discriminator, PSD - pulse shape discriminator, Co - fast overlap coincidence, Del - analog delay, GG - gate generator, TAC - time-to-amplitude converter, ADC - amplitude-to-digital converter, QDC - charge-to-digital converter, I/O - input/output register interrupt and dead time handling, S_i - scalers.*

amplifier(ORTEC 4700) and goes to the constant fraction timing discriminator (Canberra 2160). One CFT output goes directly to the overlap coincidence, the second is delayed and stops the time-to-analog converter (Canberra 2043). Its analog output is digitalized in the CAMAC ADC (Polon 712). The second output of the timing amplifier is fed to

the input of the CAMAC charge-to-digital converter (Gan'elec 1612F) which was used to determine the shape of the HPGe signal by integrating in gates of two different lengths. By measuring the shape of the HPGe signal we intended to correct for the time walk caused by different charge collection times in the large HPGe and so improve the timing resolution. In this study, however, the time correction was not yet applied. Analog signal of the α detector was fed to the second input of the QDC to measure energy of the α particles.

Pulses from the neutron detectors were processed by the pulse shape discriminator (Canberra 2160A) and the constant fraction timing discriminator. The rate of the n$\times\alpha$ coincidences was determined by TDC(Canberra 1443) with single channel analyzer output adjusted on the prompt peak. All signals important for monitoring purposes, i.e. $\alpha, \gamma \times \alpha$, n and n$\times\alpha$, were counted in 100 MHz CAMAC scalers.

Our CAMAC system was interfaced via the HYTEC 1330 crate controller to the IBM PC/AT personal computer, where an on-line program for the data acquisition was running. [8]. This program allowed simultaneously the following:

- take data from defined CAMAC modules (in our experiment 4 converters and 4 scalers). The readout cycle was started by an accepted LAM signal that simultaneously raised the dead-time flag,
- write the data on an event-by-event basis in the list mode into two ping-pong data buffers located in the high memory of the personal computer,
- write automatically filled buffers into a file on the local disk,
- create and fill requested spectra from input data stream, and
- display the requested spectra.

The list mode data files were transferred after the experiment via the ethernet computer network to the disc of the remote computer IBM/RS6000.

In the off-line analysis, data were rewritten into a N-tuple form [9] and then analysed by a powerful analysis package PAW developed at CERN [9]. In the first step we looked at the time spectrum that shows a prompt coincidence peak superimposed on the random background. Then, the limits of the prompt peak as well as two background regions on both sides of the peak were determined. The background regions were choosen in such a way that the random area under prompt peak and sum of two random background windows were identical. In the next step a net energy spectrum from the N-tuple was formed by adding events in the prompt time window and subtracting events in the both background time windows. The net energy spectrum was analysed afterwards in a classical manner.

2.4 Oxygen sample and the course of the experiment

From the very beginning we searched for a suitable oxygen sample to perform relative rather than absolute cross section measurement. We needed sample with an additional element for which a photon production cross section is well known and easy to measure.

The ratio of oxygen and reference element should be also reasonable in order to get faworable statistics for all photons detected. We have chosen CrO_3 sample for the following 2 reasons:

- the cross section for the production of the 1434.1 keV γ line from $^{52}Cr(n,n'\gamma)$ is known to be (847±23) mb, i.e. with uncertainty of only 2.7% [5],
- CrO_3 is a chromium compound with the highest oxygen content.

Our sample consisted of 147 g of CrO_3 in a powder form which was filled in the polyethylene flask with dimensions of ϕ46 mm×60 mm. The polyethylene itself does not contain oxygen, so no correction in this respect was necessary. However, after the experiment we measured the water content in our powder sample and found that it contained 0.4% of water by weight. We corrected our result for this additional oxygen content in the sample.

At an early stage of the experiment we performed a test measurement to see the detector performance at high photon energy as well as background level and performance of the whole setup. In this test experiment we used slightly different geometry than in the final measurement with the CrO_3 sample at a larger distance from the TiT target, HPGe detector at the angle of 90° and with the energy scale up to about 7 MeV of the γ energy. In this setup we irradiated the sample and measured the γ spectrum for 26 hours.

In the final measurement, we moved our sample and detector closer to the TiT target to increase the neutron flux density at the sample and moved the HPGe detector to the angle of 125° (see setup described in 2.1). In this geometry we have slightly higher random background, but our net count rate was increased. The energy range of HPGe detector was also reduced to get optimal energy $\approx$ 0.5 keV per channel. Total irradiation time in the final experiment was 50 hours.

3 Qualitative analysis of the γ spectrum

3.1 Basic features

The high energy part of the γ spectrum obtained in the test experiment at 90° is shown with all identified structures in Fig.4. Correct interpretation and analysis of this structures is crucial for several photon production cross sections in the (n,$\alpha\gamma$) channel. At the high energy end, the spectrum is dominated by the 6129 keV γ line from the inelastic neutron scattering on ^{16}O. High efficiency of our HPGe detector for high energy photons is demonstrated by the fact that the full energy peak is more intense than both single and double escape peaks even at this very high photon energy. Both γ lines at 3684 keV and 3853 keV from the $^{16}O(n,\alpha\gamma)^{13}C$ reaction are also clearly seen. Next characteristic feature in the spectrum are broad structures in the whole energy range. Some of these structures can be identified as Compton edges of various peaks.

To identify and analyse the other structures, we have to keep in mind that our reaction system is very light and the recoil velocity of the reaction product can therefore reach rather high values, usually not observed at so low incident energies. Together with very short lifetimes of several populated levels this may result in Doppler broadening of γ

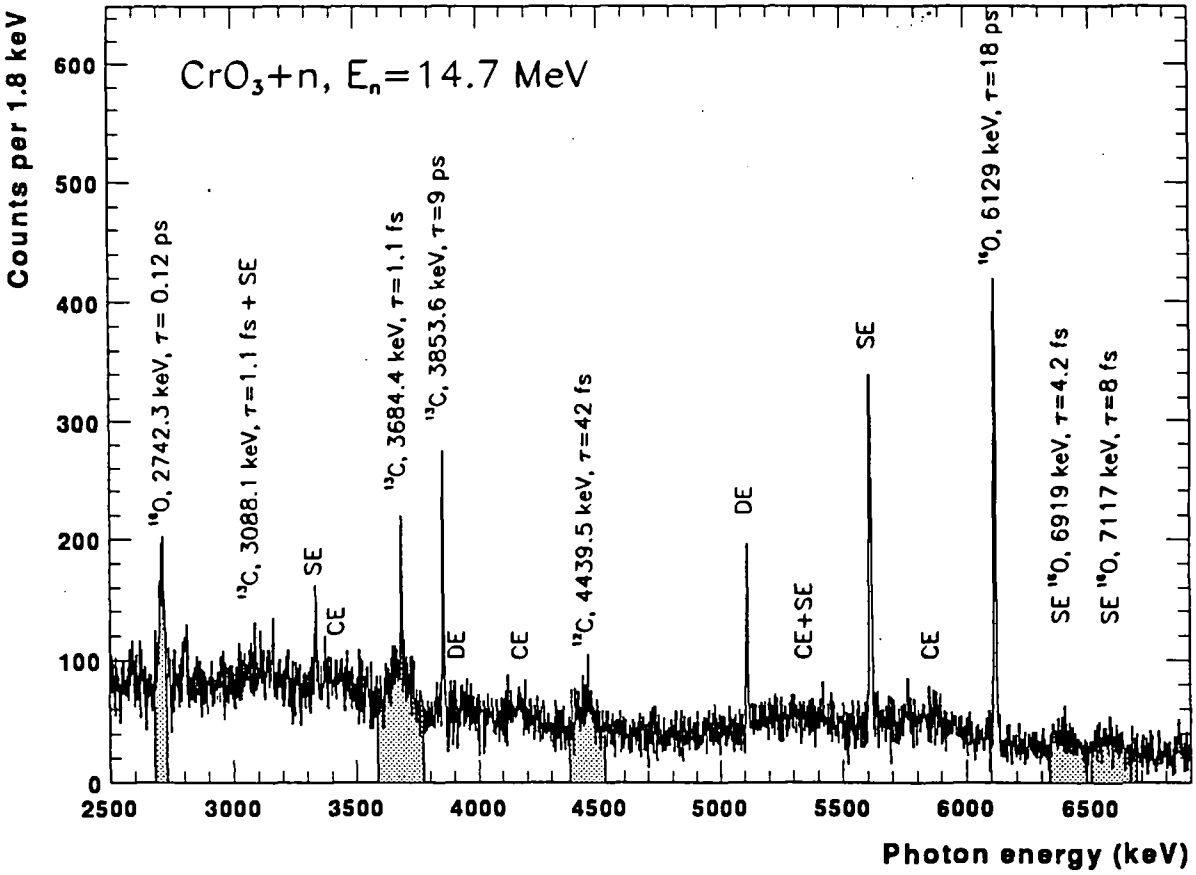

Figure 4: *High energy part of the γ spectrum obtained in the test experiment at 90°. Observed sharp peaks and broad structures in the spectrum are identified according to their origin, CE, SE and DE denote the Compton edge, single and double escape peaks, respectively. Hatched regions mark Doppler broadened peaks. For each identified γ peak the lifetime of the initial level is indicated.*

lines which depopulate these levels. Detailed analysis of Doppler broadening is rather complicated, nevertheless, on the basis of our measured spectrum we can make several conclusions discussed below.

3.2 Doppler broadening

The Doppler broadening can be observed when photons are emitted from a moving nucleus. This may occur when the velocity of the emitting nucleus is high and the lifetime of the nuclear level is shorter than the stopping time of the recoiling nucleus. In the spectrum on Fig.4 we can see several broad structures, that we identify as γ peaks with various degree of Doppler broadening. The width of the broadened peak depends not only on the lifetime of the corresponding level, but also on the feeding pattern of this level.

Here we are not able to make a quantitative discussion of the Doppler broadening for reasons which will be clarified soon, but we start our qualitative analysis with a simple case of a nuclear level which is populated only by particle feeding. In this case the average Doppler shift $\overline{\Delta E_\gamma}$ can be expressed as [6]

$$\overline{\Delta E_\gamma} = F(\tau) E_\gamma \beta_r \cos(\theta), \tag{2}$$

where E_γ is emitted photon energy, β_r is the recoil velocity in units of c, θ is the observation angle and $F(\tau)$ is the function which takes into account stopping of the recoiling nucleus as well as the lifetime of the decaying level.

It is the function $F(\tau)$ which prevents quantitative analysis of the Doppler broadening in our case, because we lack experimental information on stopping of ^{13}C in the heterogenous CrO_3 sample. In the very simple case of the homogeneous sample this function may be approximated by [6]

$$F(\tau) = \frac{\alpha}{\alpha + \tau}, \tag{3}$$

where α is here the average stopping time with a typical value $\alpha \sim 0.1$ ps and τ is the lifetime of the level. For our case of the powder sample, we may expect for α somewhat higher values. From the velocity of incident neutrons and the mass of the target we get $\beta \sim 0.01$ for the recoil nucleus which gives maximal Doppler shift of $\approx$40 keV for a photon of 4000 keV energy. The Doppler broadening may reach up to more than twice of this value, depending on the kinematics of the reaction including also angular distribution of emitted α particles. The Doppler broadening can be observed only for levels with lifetime shorter than $\approx$ 0.1 ps. For γ lines depopulating levels with longer lifetime there will be no observable broadening.

The above picture is valid only in the case of direct particle feeding of the level in question. When the level is feeded by γ decay from higher levels, the broadening depends on lifetimes of these levels. For instance, when a short-lived level is feeded from a level with a long lifetime we will not observe any broadening since photons are emitted from the nucleus already at rest.

In our γ spectrum we see the sharp peak at 6129 keV as well as its single and double escape peaks from the inelastic neutron scattering on ^{16}O. The lifetime of the 6129 keV level of ^{16}O is τ= 18 ps and according to our simple picture one should not observe any broadening in this case, because of $\tau \gg \alpha$. The next prominent peak is at 3853 keV and its single escape comes from the decay of the 12.5 ps level in ^{13}C and it is also sharp.

All other observed peaks show some broadening. The peak at 2742 keV we identify as the $2^- \rightarrow 3^-$ transition in ^{16}O, where the lifetime of the 2^- level is τ= 0.12 ps, the value at which we should start to observe the Doppler broadening. This is actually the case, because of the width of this peak is several times higher than the intrinsic resolution of our detector at this energy.

The broad structure at 4440 keV we identify as the Doppler broadened γ transition $2^+ \rightarrow 0^+$ from $^{16}O(n,n'\alpha)^{12}C$. The lifetime of the 2^+ level at 4439.5 keV is only 42 fs and the observed broadening is rather high. Next two broad structures in the observed spectrum are peaks near 6408 and 6608 keV which we identify as single escape peaks from 6919 and 7117 keV γ transitions. They depopulate levels with lifetimes of 4.2 fs and 8 fs, respectively and because of this short lifetime the both peaks are broad.

The structure at 3684 keV, which we identify as the full energy peak from the $3/2^- \rightarrow 1/2^-$ transition in the $^{16}O(n,\alpha\gamma)^{13}C$ reaction shows a peculiar shape. A rather sharp part with apparently no broadening is superimposed on a broad structure. This is an example of a more complicated feeding of the $3/2^-$ level with the lifetime of only $\tau = 1.6$ fs. Here, $\tau \ll \alpha$ and in the case of simple particle feeding we should observe a very broad peak. In addition, the $3/2^-$ level is feeded by the γ transition from the $5/2^+$ level at 3853.6 keV with the lifetime of 12.5 ps [14]. This part of intensity is sharp, similarly to the 3853.6 keV γ transition itself, because the lifetime is in this case effectively determined by the decay of the long-lived level $5/2^+$. Unfortunately, we were not able to observe the $5/2^+ \rightarrow 3/2^-$ transition experimentally because of its very low energy of 169 keV.

By thorough inspection of Fig.4 one can identify a small broad structure at $\approx$ 3100 keV. This may correspond to the 3088 keV $1/2^+ \rightarrow 1/2^-$ transition from the $^{16}O(n,\alpha\gamma)^{13}C$ reaction. The lifetime of the 3088 keV level in ^{13}C is also very short, 1.5 fs, therefore we expect rather strong Doppler broadening, similar to the 3684 keV transition. Unfortunately, this structure is masked by the single escape peak from the broadened 3684 keV transition, which together with the apparent weakness of the 3088 keV γ transition makes its positive identification difficult.

All other broad structures in the spectrum can be explained by the response of our HPGe detector as Compton edges of various full energy peaks.

To summarize our analysis of the high energy part of the spectrum, we see that the Doppler effect plays an important role in the γ spectrometry of the very light systems. In our special case of the $^{16}O(n,\alpha\gamma)^{13}C$ reaction one should take these effects into account especially in the analysis of the 3684.4 keV transition.

4 Results and Discussion

4.1 Peak areas

The observed γ ray energy spectrum with random background subtracted is shown in Fig.5. The most prominent peak is 1434 keV from the reference reaction $^{52}Cr(n,n'\gamma)$. Both high energy peaks 3684.4 and 3853.6 keV from the reaction $^{16}O(n,\alpha\gamma)^{13}C$ are visible at the right hand side of the spectrum. There are many others peaks in the spectrum, mainly in the low energy region. The majority of them originated in the neutron interactions with Cr. Broad structures with asymmetric shapes around 600 and 800 keV are from interactions of elastically scattered neutrons with Ge in the HPGe itself. The broadening is caused by absorption of recoil energy in the HPGe crystal. We were not able to determine any significant intensity which would correspond to the low energy transitions between excited levels of ^{13}C, i.e., 596 and 765 keV.

We determined areas of all peaks by the simple algorithm in which we selected the peak region and two background regions on both sides of the peak in question. Then, we integrated the peak region and determined background by linear interpolation of two background windows. We used this procedure for all narrow peaks, i.e., for 1443.1 keV, 3853.6 keV and the narrow part of the 3684.4 keV transition. Very difficult task was the area determination of the broadened 3684.4 keV transition. Although the whole procedure is the same as for narrow peaks, the difficulty arise with setting of both background and

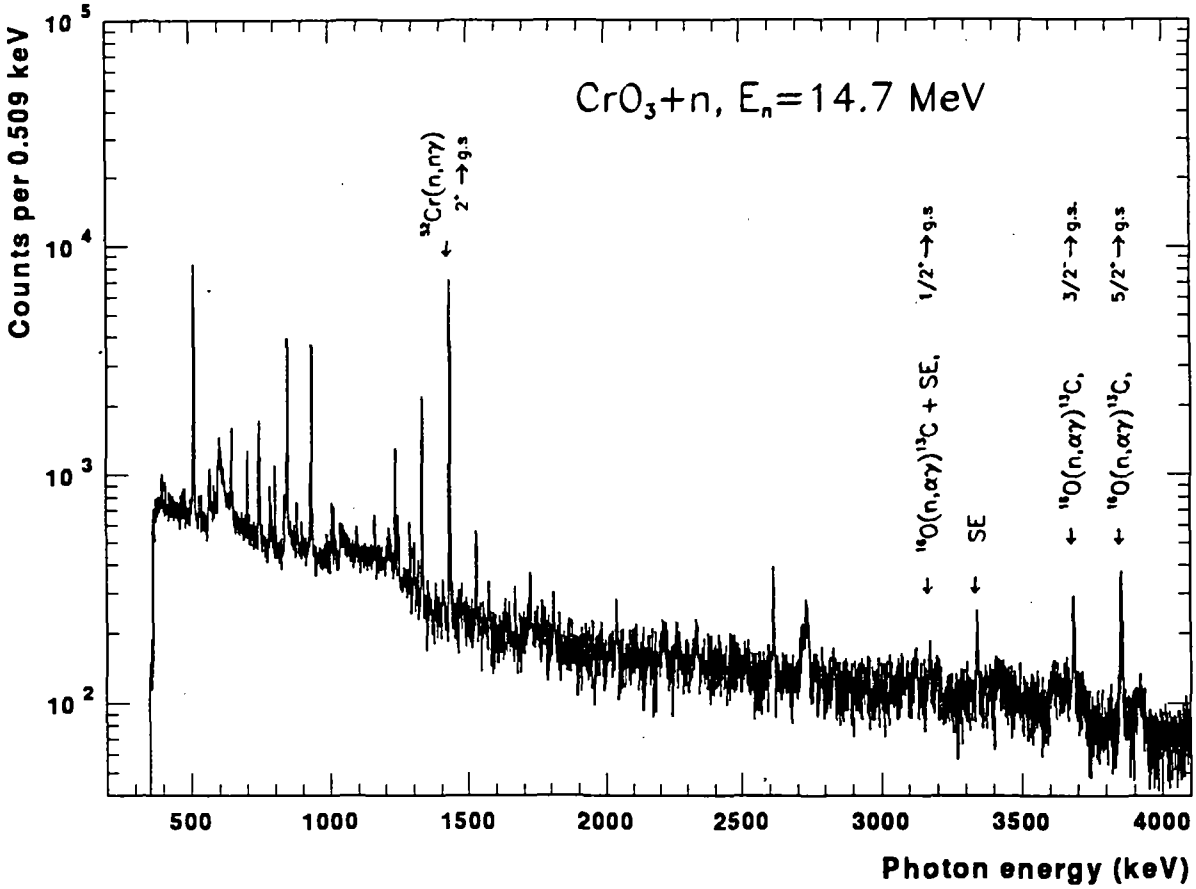

Figure 5: *Net energy spectrum obtained in the CrO_3+ n experiment after subtraction of random background. Only full energy peaks relevant for the cross section determination are labeled in this spectrum.*

peak regions. Typical background setting is shown in detail in Fig. 6. The background under the peak itself was assumed to be linear and it is shown as a line. According to our previous discussion we assume that the broadened part corresponds to the direct particle population of the $3/2^-$ level at 3684.4 keV in the ^{13}C and the sharp fraction of the full energy peak corresponds to the population via 169.2 keV transition from the $5/2^+$ level.

More difficult is an attempt to determine the cross section for the production of the 3088.4 keV γ ray transition. Lifetime of this $1/2^+$ level is 1.5 fs, the same as the lifetime of the 3684.4 keV level. Therefore, this transition should also be broadened. Moreover, in this region falls also the single escape peak of the broadened 3684.4 keV γ ray. The final energy spectrum in Fig.5 shows a structure in this region which seems to support our interpretation. Measured efficiency of single escape peak shows that the majority of this intensity corresponds to the single escape peak of 3684.4 keV. We determined this part of the observed intensity from the peak area and the single escape peak efficiency of the 3684.4 keV transition. The intensity corresponding to the 3088.4 keV transition

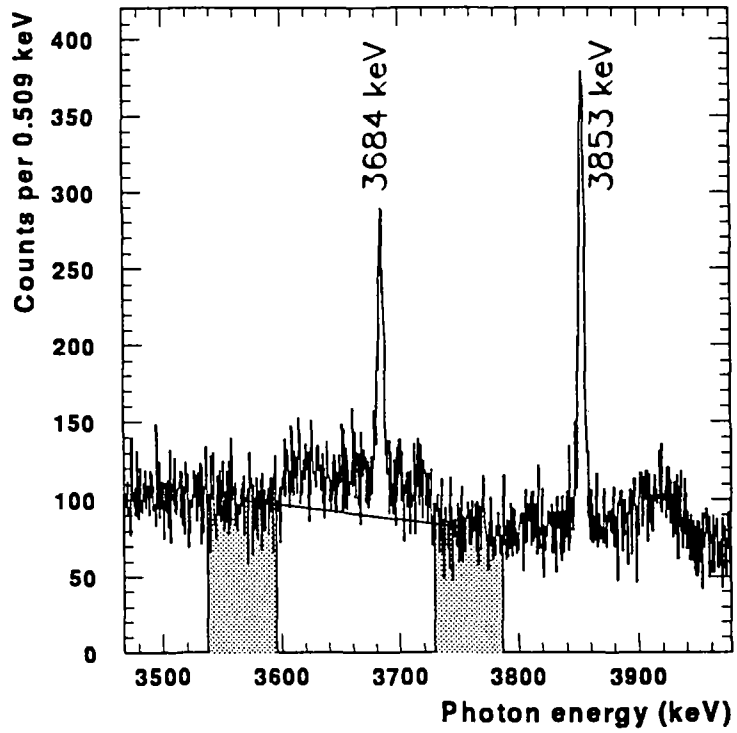

Figure 6: *High energy part of the γ ray spectrum with 3684.4 and 3853.6 keV transitions. Hatched regions were used for the background determination (see the straight line) under the broadened 3684.4 keV peak.*

was determined as the difference between the area of the structure near 3100 keV and the calculated intensity corresponding to the single escape peak of 3684.4 keV.

The uncertainties of the peak areas were calculated as sum of statistical peak and background uncertainties. For the broadened 3684.4 keV and 3088.4 keV transition we added an additional term, which should account for somewhat subjective setting of peak and background regions. We determined the net peak area for different peak and window regions. From peak area variation for different region settings we got a systematic error, which we added geometrically to the statistical errors. The final uncertainties of the peak areas (see Tab.4.1) vary between 0.5% and 18% for 1434.1 keV and 3088.2 keV γ transition, respectively.

Experimentally determined areas net areas of the relevant peaks in both ^{13}C and ^{52}Cr are summarized in Tab.4.1. Relative full energy peak efficiences of the HPGe detector are also given in this table.

Cross sections were determined relatively to the cross section of the 1434.1 keV transition using the following formula

$$\sigma_i = \frac{N_i \times \epsilon_{1434} \times C_{1434} \times f_i \times n_{^{52}Cr}}{N_{1434} \times \epsilon_i \times C_i \times f_{1434} \times n_{^{16}O}} \times \sigma_{1434}, \qquad (4)$$

where i= 3684,3853, σ_i is the cross section in (mb), N_i is peak area in the observed

Transition energy(keV)	Reaction	Area	Rel. Efficiency
1434.1	^{52}Cr(n,n'γ)	52209±257	1.000
3088.0	^{16}O(n,$\alpha\gamma$)	510±90	0.589±0.029
3683.8	^{16}O(n,$\alpha\gamma$)	8486±428	0.521±0.026
3853.6	^{16}O(n,$\alpha\gamma$)	3573±174	0.504±0.025

Table 1: *Peak areas of relevant peaks extracted from the experimental spectrum and the relative full energy peak efficiences.*

spectrum, C_i is the correction for γ ray absorption in the sample, f_i is correction factor for secondary neutron contribution, ϵ_i is the relative full energy peak efficiency and n_A is the number of indicated nuclei in the sample.

The cross section for the production of the 1434.1 keV γ ray was based on the data given in Ref. [5]. The isotopic cross section of 924±25 mb at 14.0 MeV was converted to 14.7 MeV using gradient of 193 mb/MeV. We corrected this cross section for the ^{53}Cr(n,2n) contribution assuming 9.5% abundance of ^{53}Cr, cross section of ^{53}Cr(n,2n) reaction of 933 mb and 85% probability for production of the 1434.1 keV γ ray in the (n,2n) reaction. For the natural mixture of Cr we got then for production of the 1434.1 keV γ ray at 14.7 MeV incident neutron energy the effective cross section of 695±28mb.

4.2 Corrections

Two kinds of corrections were applieded, according to the Eq. (1). The first one is the simple correction for photon selfabsorption in the sample. The mean photon path in the sample was calculated using the Monte Carlo technique. We reduced the photon attenuation coefficients of Ref. [10] to account for reduced density of our powder sample.

The second correction accounts for effects of secondary neutrons in the sample. Secondary neutrons are produced in the sample by inelastic scattering and their energy is lower than the incident energy of 14.7 MeV. Excitation curves for both reference (n,n'γ) and (n,$\alpha\gamma$) reactions are rather complicated function of incident energy. In general, secondary neutrons have higher probability of producing inelastic γ rays, in our case especially the 1434.1 keV γ line than do the 14.7 MeV neutrons. The oposite is true for γ rays from (n,α) reaction because of high Q-value of this reaction. For calculation of this correction, we followed the development at IRK Vienna [11] and used the following formulas

$$f_i = 1 - \frac{N_{sec}}{N_{prim}} \tag{5}$$

$$\frac{N_{sec}}{N_{prim}} = \frac{n \times \bar{l} \times \int_0^{E_0} \frac{d\sigma(E_0,E_{n'})}{dE_{n'}} \sigma_{\gamma_i}(E_{n'}) dE_{n'}}{\sigma_{\gamma_i}(E_0)}, \tag{6}$$

where f_i is the correction for secondary effects, $d\sigma(E_0,E_{n'})/dE_{n'}$ is differential production cross section for secondary neutrons of energy $E_{n'}$ by primary neutrons of energy E_0,

$\sigma_{\gamma_i}(E_{n'})$ is the production cross section for photons of energy E_γ by secondary neutrons of energy $E_{n'}$, $\bar{l}$ is the average path of secondary neutrons in the sample and n is the number of the nuclei per 1cm^3. All differential and production cros sections sections for this formula were taken from evaluated nuclear data library ENDF/B-VI.

Photon energy E_i (keV)	Selfabsorption C_i	Multiple scattering f_i
1434.1	0.96	0.89
3088.4	0.97	0.92
3684.4	0.98	0.91
3853.6	0.98	0.91

Table 2: *Multiple scattering and selfabsorption corrections used in data evaluation.*

The corrections applied for each individual γ transition are summarized in Tab.4.2. The estimated uncertainty of the total correction is 3%.

Energy (keV)	Transition	Cross section (mb)
3088.4	$1/2^+ \rightarrow 1/2^-$	3.1±0.6
3684.4	$3/2^- \rightarrow 1/2^-$	53.5±5.0
3684.4[a]	$3/2^- \rightarrow 1/2^-$	13.0±1.2
3853.6	$5/2^+ \rightarrow 1/2^-$	24.3±2.2

[a]unshifted part corresponding to the γ feeding from the $5/2^+$ level

Table 3: *Cross sections for the production of discrete γ transitions in the $^{16}O(n,\alpha\gamma)^{13}C$ reaction at 14.7 MeV. Given are also cross section for production of 3088.4 keV transition as well as cross section for indirect production of the 3684.4 keV transition.*

Uncertainty in the relative full energy peak efficiency was estimated to be 5% for photon energies above 3000 keV. The uncertainty in the correction factor is given by the uncertainty for the secondary effects and was estimated to be 3%. The error in the selfabsorption term was neglected, because the mean absorption length was calculated with accuracy better than 1%. The cross sections calculated according to the formula 4 are given together with final uncertainties in Tab.3.

4.3 Discussion

The cross section of the 3684.4 keV γ transition is strongly influenced by the interpretation of the peak shape. Our interpretation is based on the observation that the peak shape is caused by complex feeding scheme of the 3684.4 keV level and Doppler broadening. This

is supported by a similar finding by Dickens and Perey [13], who observed Doppler effects in $^{16}O(n,\alpha\gamma)$ reaction at still lower incident neutron energies between 6.4 and 10.6 MeV.

In addition, this is strongly supported by the spectroscopic information on γ decay branching of the $5/2^+$ level. According to Warburton [14], the $5/2^+$ level decays with the

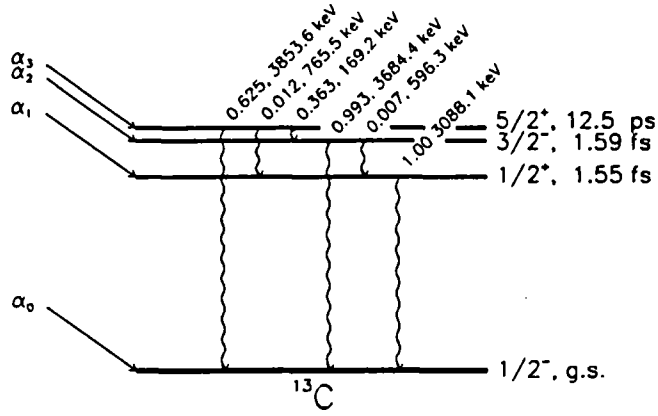

Figure 7: *Simplified level scheme of ^{13}C with γ ray branching ratios taken from Ref. [14].*

probability of (62.5±0.6)% to the ground state and with the probability of (36.3±0.6)% to the $3/2^-$ level at the 3684.4 keV, see Fig.7. It appears that we can calculate this branching ratios from our cross section data. An agreement of branching calculated from our cross sections with literature data would represent a strong argument in favor of our interpretation. The γ branch going through the $3/2^-$ level is given as the ratio of the cross section of the sharp part of the 3684.4 keV transition σ_{3684}^{sharp} to the total population of the $5/2^+$ level $\sigma_{5/2^+}$. One has

$$b = \frac{\sigma_{3684}^{sharp}}{\sigma_{5/2^+}} = \frac{\sigma_{3684}^{sharp}}{\sigma_{3853} + \sigma_{3684}^{sharp}} = 0.346 \pm 0.039. \quad (7)$$

This value is in excellent agreement with the spectroscopic measurement [14].

The complex shape of the 3684.4 keV γ line allows also to determine the discrete level population in the (n,α) reaction and therefore perform direct comparison with charged particle cross section data. The population of $5/2^+$ and $3/2^-$ levels is (37.5±2.5) mb and (40.9±5.3) mb, respectively.

Both $5/2^+$ and $3/2^-$ levels have weak γ decay branch to the $1/2^+$ level at 3088.8 keV with branching ratios of 1.2 % and 0.7%, respectively [14]. For production of the 3088.8 keV transition we measured cross section of (3.1±0.6) mb, from which 0.6 mb represents contribution from γ branching from higher levels and for direct α particle population is left only (2.5±0.6) mb.

Total α particle production cross section is given by the sum of all partial level populations. Naturally, in our method we can not account for direct ground state population. For the total population of excited states in ^{13}C we get

$$\sigma_{\alpha^*} = \sigma_{3684} + \sigma_{3853} + \sigma_{3088} = (53.5 \pm 5.0) + (24.3 \pm 2.2) + (3.1 \pm 0.6) = (80.9 \pm 5.4)\ mb. \quad (8)$$

However, using experimental cross section for the α_0 branch [3] of 17.3±3.4 mb for g.s. population, we can estimate from our γ production cross section the total α production cross section to be

$$\sigma_\alpha = \sigma_{\alpha_0} + \sigma_{\alpha^*} = (80.9 \pm 5.4) + (17.3 \pm 3.4) = (98.8 \pm 6.4)\ mb \qquad (9)$$

We can now compare our results with the literature data, starting with the γ production. The γ production cross section of 3684.4 transition measured in this work is compared with known experimental data [15] in Fig.8 All these data are rather old and

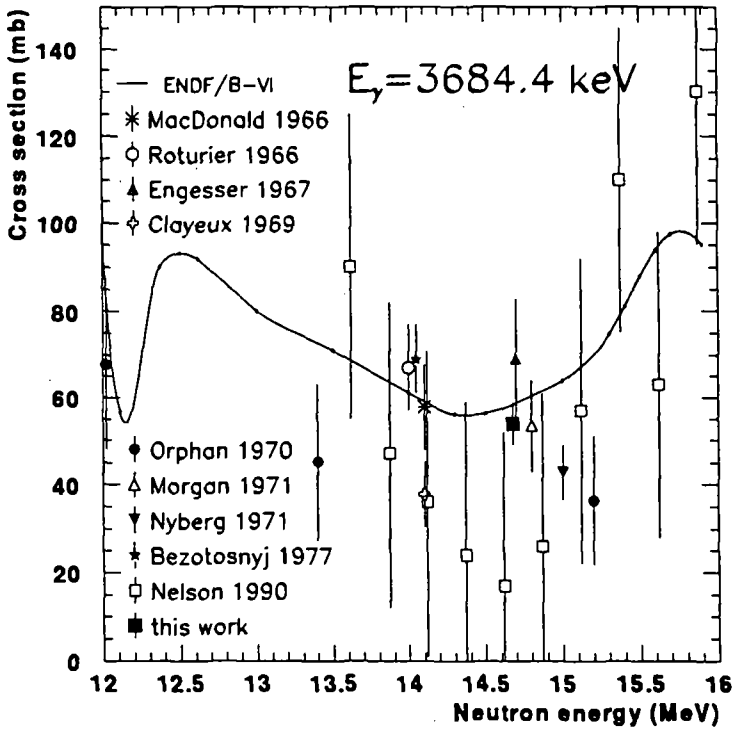

Figure 8: *Cross section for production of 3684.4 keV γ transition in the $^{16}O(n,\alpha\gamma)^{13}C$ reaction between 12 and 16 MeV incident neutron energy. Our result is compared with existing experimental data (see list in Ref. [15]. The smooth line is a spline polynomial connecting evaluated points from ENDF/B-VI.*

majority of them were obtained with low resolution NaI(Tl) detectors. Only 5 measurements were performed using high resolution Ge(Li) detectors. Of them four older measurements by Orphan, Clayeux, Nyberg and Yamamoto were handicapped by rather low efficiency of early semiconductor detectors with the active volume almost one order of magnitude lower than today available HPGe detectors. Only Nelson offer new data taken with a large Ge(Li), his data show in the 14 MeV region rather strong energy dependence and their uncertainties are also fairly large. Other literature data for production of this γ line show also large spread between 38 and 62 mb . Our value of 53.5±5.0 mb therefore represents an almost mean value of the older experimental data.

The origin of the differences is not completely understood. Neglecting the Doppler broadened part of the peak results in a substantial reduction of the peak intensity and lead to the low value of cross section. However, this is relevant only for measurements with high resolution Ge spectrometers and not for NaI(Tl) detectors, where this effect could not be

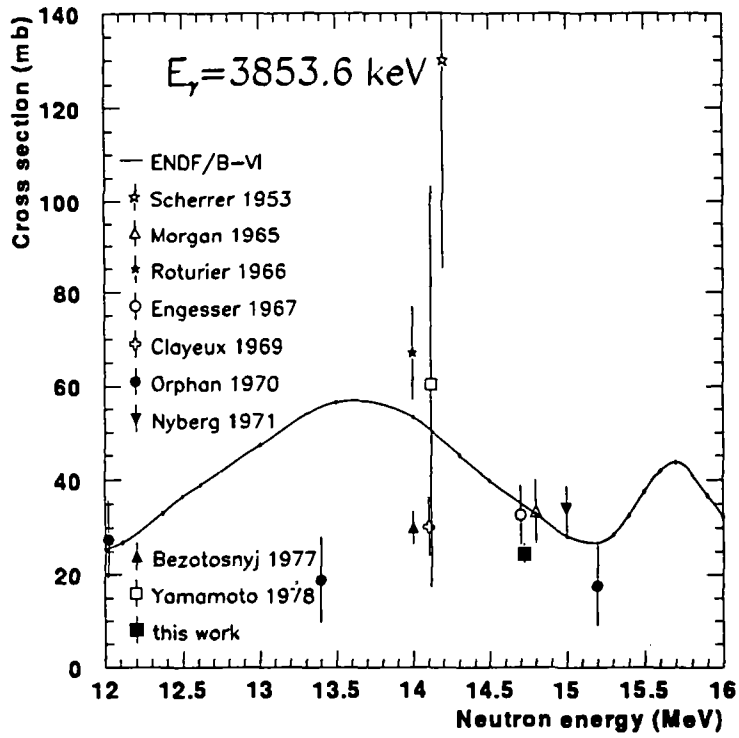

Figure 9: *Cross section for 3853.6 keV γ transition production in the $^{16}O(n,\alpha\gamma)^{13}C$ reaction. Our cross section is compared with other literature data and ENDF/B-VI evaluation between 12 and 16 MeV incident neutron energy. The smooth line is a spline polynomial connecting points given by ENDF/B-VI.*

observed. Part of the differences may be explained because of our improved experimental technique, large HPGe detector with very good energy resolution and setup with relatively low background. Relative cross section measurement also removed uncertainties usually connected with absolute neutron flux and detection efficiency determination. With respect to the evaluated data, our experimental point is slightly lower than the ENDF/B-VI value of 60.4 mb at 14.8 MeV.

The literature data [15] for the 3853.6 keV γ line production are summarized together with our result in Fig.9. The experimental data may be divided into two parts. The first group scattered around ~30 mb represent the part with less dispersion and lower values. Measurements by Scherrer and Yamamoto show rather large uncertainties and their values are substantially higher than the other group. Our measurement supports the former group with lower cross sections. Origin of the discrepancies is not known. However, the Scherrer measurement is rather old and was performed with very low resolution NaI(Tl)

spectrometer. The result given by Yamamoto is relatively new, but its uncertainty is so high that it is even in accord with other measurements. Our experimental value (24.3±2.2) mb is here again somewhat lower than the ENDF/B-VI evaluation, which gives cross section of 32.7 mb at 14.7 MeV.

Total discrete γ production measured in the present work is (80.9±5.5) mb. To compare this value with the total α particle production, we added ground state population from measurement of Borman [3]. We got then for total α particle production cross section of (98.2±6.4) mb. This value is lower than the cross section accepted in the ENDF/B-VI evaluation for the total α particle production, which is 131.7 mb. On the other hand, our value is in accord with the JENDL-3 evaluation which gives at 14.6 Mev cross section of 99.4 mb.

5 Conclusions

We measured discrete cross section of γ ray production cross sections in the $^{16}O(n,\alpha\gamma)^{13}C$ reaction at 14.7 MeV. We used large HPGe detector, up-to date electronics and computerized multiparametric data acquisition system. Cross sections were determined relatively to the well known reference $^{52}Cr(n,n'\gamma)$ reaction with precission better than 10%. We found that Doppler effects play an important role in this very light system. For the short–lived $3/2^-$ level we accounted for this fact and arrived at the cross section that is comparable roughly to the mean value of other known experimental data around 14 MeV. We determined the total discrete γ ray production to be (80.9±5.4) mb and we deduced the total ^{16}O $(n,\alpha)^{13}C$ cross section of (98.9±6.4)mb. This later value is lower than the other experimental data as well as the ENDF/B-VI evaluation, it is, however in excellent agreement with the JENDL-3 evaluation.

Acknowledgement

We are gratefull to H. Vonach for suggesting us this measurement. We would like to thank E. T. Cheng for his kind support and interest. O. Schwerer provided us with help in using EXFOR and the on-line information services of the IAEA Nuclear Data Section (NDIS). We thank A. B. Pashchenko for the support and interest. This work was supported in part by the International Atomic Energy Agency Research Contract No. 6970 and by the Grant of the Slovak Academy of Sciences No. 042/92.

References

[1] H. Vonach, IRK Vienna, private communication, June 1992

[2] J. Pivarč and S. Hlaváč, Nucl. Sci. Eng. 106 (1990) 266.

[3] M. Borman, Z. Physik 258 (1973) 285.

[4] S. Hlaváč, P. Obložinský, I. Turzo, L. Dostál, H. Vonach, A. Pavlik and S. Simakov, submitted to Nucl. Sci. Eng.

[5] H. Vonach, S. Tagesen, M. Wagner and A. Pavlik, Physics Data 13-6, (Fachinformationszentrum Karlsruhe 1991).

[6] A. Morinaga and Y. Yamazaki, In Beam γ-ray Spectroscopy, (North Holland, Amsterdam 1975) p. 410.

[7] C. M. Lederer and V. S. Shirley, eds.,Table of Isotopes, (J. Wiley & Sons, New York 1978).

[8] M. Morháč, I. Turzo and J. Krištiak, PC-CAMAC based data acquisition system for multiparametric measurements, Proc. 8th Conf. on Real-Time Computer Applications in Nuclear, Particle & Plasma Physics, (Vancouver, June 1993) p.220.

[9] Application Software Group, PAW - Physics Analysis Workstation, CERN Program Library Entry Q121, (CERN, Geneva 1993).

[10] D. E. Cullen, M. H. Chen, J. H. Hubbell, S. T. Perkins, E. F. Plechaty, J. A. Rathkopf and J. H. Scofield, Report UCRL-50400, Vol. 6, Part A, Rev. 4, (LLNL Livermore 1989).

[11] A. Pavlik, IRK Vienna, Private communication, May 1993.

[12] V. J. Orphan C. G. Hoot and J. John, Nucl. Sci. Eng. 42 (1970) 352.

[13] J. K. Dickens and F. G. Perey, Nucl. Sci. Eng. 40 (1970) 283.

[14] E. K. Warburton, D. E. Alburger and D. J. Millener, Phys. Rev. C22 (1980) 2330.

[15] Literature data for production of 3684.3 and 3853.6 keV γ lines:

- **Scherrer 1953**—V. E. Scherrer, R. B. Theus and W. R. Faust, Phys. Rev. 91 (1953) 1476, EXFOR 11306.
- **McDonald 1966**—W. J. McDonald, J. M. Robson and R. Malcolm, Nucl. Phys. 75 (1966) 353, EXFOR 11383.
- **Roturier 1966**— J. Roturier, Compt. Rendu 262 (1966) 1736, EXFOR 20599.
- **Engesser 1967**— F. Engesser and W. Thompson, J. Nucl. Energy 21 (1967) 487, EXFOR 11531.
- **Clayeux 1969**— J. Clayeux, Report CEA-R-3807, EXFOR 21677.
- **Morgan 1969**— I. L. Morgan, J. B. Ashe and D. O. Nellis, Oak Ridge Report ORO-2791-32, 1971, EXFOR 12695.
- **Orphan 1970**— V. J. Orphan, C. G. Hoot and J. John, Nucl. Sci. Eng. 42 (1970) 352, EXFOR 10097.
- **Nyberg 1971**— K. Nyberg-Ponnert, B. Jönsson and I. Bergqvist, Phys. Scripta 4 (1971) 165, EXFOR 20245.
- **Bezotosnyj 1978**— V. M. Bezotosnyj, V. M. Gorbachev, M. A. Efimova, L. M. Surov and M. S. Shevcov, Yad. Konst. 30 (1978) 21, EXFOR 40516.

- **Yamamoto 1987**—T. Yamamoto, Y. Hino, S. Itagaki and K. Sugiyama, J. Nucl. Sci. Techn. 15 (1978) 797, EXFOR 21304.
- **Nelson 1990**— R. Nelson, Proc. Washington Conf. Nucl. Data 1990.
- **ENDF/B-VI**— G. Hale, Z. Chen and P. Young, Evaluation of ^{16}O for ENDF/B-VI, LANL 1990.